Markedly Enhanced Permeability and Retention Effects Induced by Photo-immunotherapy of Tumors

Kohei Sano, Takahito Nakajima, Peter L. Choyke, and Hisataka Kobayashi*

Molecular Imaging Program, Center for Cancer Research, National Cancer Institute, National Institutes of Health, Bethesda, Maryland 20892-1088, United States

ABSTRACT A major barrier to cancer treatment is the inability to deliver sufficient concentrations of drug to the tumor without incurring systemic toxicities. Nanomaterials are appealing because they can carry a large drug payload; however, tumor delivery is limited by modest leakage and retention in most tumors. We observed that after photoimmunotherapy (PIT), which is a light-mediated treatment based on an antibody—photosensitizer conjugate, there was surprisingly high leakage of nanosized (10—200 nm) agents into the tumor bed. PIT rapidly induced death in perivascular cancer cells, leading to immediate and dramatic increases in vascular permeability, resulting in up to 24-fold greater accumulation of nanomaterials within the PIT-treated tumor compared with controls, an effect termed "super-enhanced permeability and retention". In a treatment study, PIT followed by liposome-containing daunorubicin, DaunoXome (diameter 50 nm), resulted in greater survival in tumor-bearing mice than either PIT or DaunoXome alone. Thus, PIT greatly enhances delivery of nanosized reagents and thus holds promise to improve therapeutic responses.

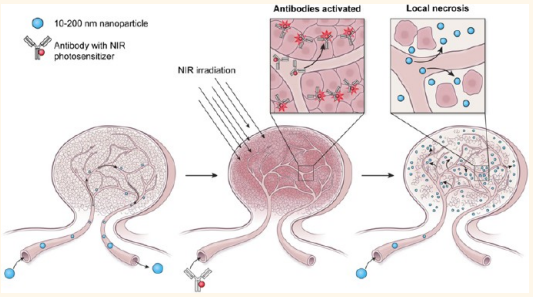

KEYWORDS: drug delivery · super-enhanced permeability and retention effect · photoimmunotherapy · nanomaterials · cancer imaging · cancer therapy

Drug delivery is a central issue in oncology. Highly toxic drugs often are not effective *in vivo* because insufficient intratumoral concentrations are achieved due to heterogeneous vascularity, high interstitial pressures, and other barrier effects.[1,2] At the same time, nontarget effects limit the dose that can be safely administered. Targeted nanosized delivery vehicles, including liposomes, nanomicelles, and nanoparticles, have been employed in the hopes of delivering more drugs per particle and relying on the enhanced permeability and retention (EPR) effect to selectively accumulate the agents.[3—6] Although the EPR effect results in improved delivery to tumors compared with normal tissue, especially for nanosized reagents, EPR is still inefficient, and only relatively low concentrations of a nanosized agent can be achieved within a tumor.[7] The most well-known nanosized preparations in clinical use are liposomal drugs such as Doxil or DaunoXome, both of which have shown efficacy that is comparable to their lower molecular weight counterparts, which require more frequent dosing.[8—10] In order to achieve superior effects with nanosized therapies, a method to further enhance their selective accumulation within tumors must be found.

Photoimmunotherapy (PIT) is a newly described cancer treatment that employs a targeted monoclonal antibody (mAb) conjugated to a photosensitizer, IR-700.[11] Upon exposure to light (690 nm wavelength), highly specific cell killing is rapidly achieved. The antibody conjugate is maximally bound to cells in the immediate perivascular space, and the rapid killing of these cells leads to immediate increases in vascular permeability, allowing the rapid leakage of nanosized particles into the tumor space. This effect can be immediately visualized using a variety of imaging methods employing labeled nanoparticles. The strikingly clear increase in permeability for nanoparticles, followed by their retention in the tumor space, has prompted us to term this effect "super EPR", or SUPR. Herein, we demonstrate the SUPR effect using a variety of imaging methods and then demonstrate how the increased delivery of nanosized liposomal chemotherapy

* Address correspondence to kobayash@mail.nih.gov.

Received for review October 28, 2012 and accepted December 7, 2012.

Published online December 07, 2012
10.1021/nn305011p

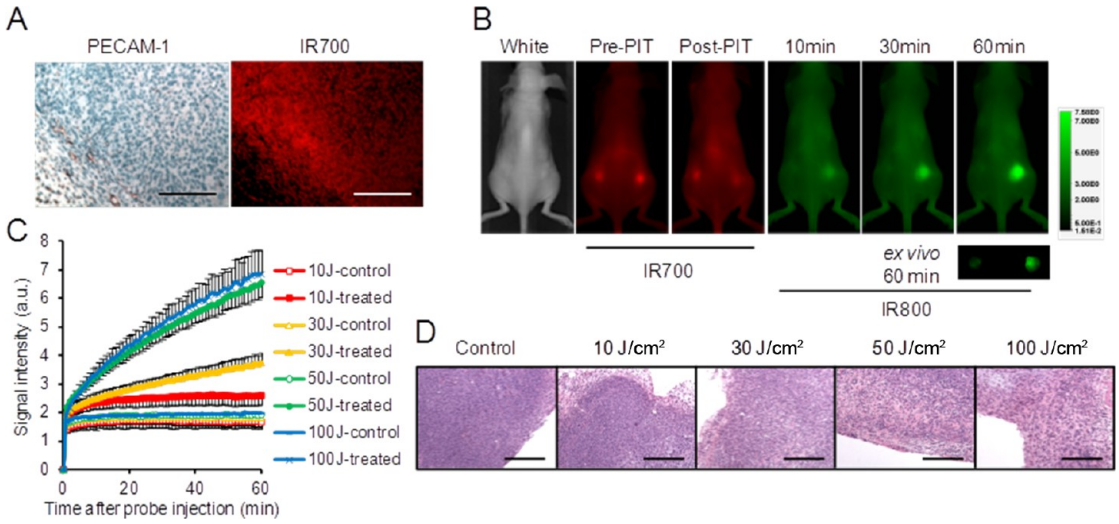

Figure 1. Biodistribution of Pan-IR800 conjugate following PIT. Mice bearing A431 tumors were initially injected with Pan-IR700, and 1 d later, NIR light (50 J/cm^2) was administered to the right tumor, while the left tumor was shielded from light. (A) Blood vessel staining (PECAM-1) and distribution of Pan-IR700 in A431 tumors. Scale bars: 200 μm. (B) Dynamic fluorescence images of Pan-IR800 after Pan-IR700-mediated PIT. Pan-IR800 was administered 1 h after PIT. Only the PIT-treated tumor (right) was clearly seen within 60 min. IR700: red, IR800: green. (C) Light dose-dependent accumulation of Pan-IR800 after Pan-IR700-mediated PIT. Data are means ± SEM (n = 4). (D) H&E staining suggested that necrotic damage after PIT was more intense with high-dose NIR light. Scale bars: 400 μm.

to PIT-treated lesions leads to improved responses in an animal tumor model.

RESULTS AND DISCUSSION

PIT-Enhanced Accumulation of Specific Antibody in Tumors. Accumulation and distribution of monoclonal antibody in the PIT-treated tumor and control tumor were investigated. Animals bearing A431 xenografts were injected with panitumumab bound to IR700 (Pan-IR700). Panitumumab is an FDA-approved monoclonal antibody directed at HER1[12] and A431 cells produce HER1-expressing tumors. One day after injection, Pan-IR700 was observed to accumulate in perivascular tumor cells, and a gradient of IR700 fluorescence signals was observed depending on the distance from blood vessels (Figure 1A). A single dose of NIR light (50 J/cm^2) was exposed to one tumor, while the contralateral tumor was shielded from light. The fluorescence signal of IR700 was decreased after PIT due to washout from necrotic cancer cells as well as some degree of photobleaching. *In vivo* fluorescence imaging of panitumumab conjugated with IR800 (Pan-IR800), administered 1 h after light irradiation, demonstrated rapid uptake of the agent within 60 min in PIT-treated tumors, while no change in signal intensity was detected in control tumors (Figure 1B and Video S1 in the Supporting Information). Light signal intensities (SIs) of Pan-IR800 in PIT-treated tumors increased with time in a light dose-dependent manner (Figure 1C), up to 50 J/cm^2. The background-corrected uptake of Pan-IR800 in PIT (50 J/cm^2)-treated tumors was 21.5-fold higher than in control tumors between 1 and 60 min after PIT using the following equation: $[(SI_{PIT\ at\ 60\ min} - SI_{Background\ at\ 60\ min}) - (SI_{PIT\ at\ 1\ min} - SI_{Background\ at\ 1\ min})]/[(SI_{Control\ at\ 60\ min} - SI_{Background\ at\ 60\ min}) - (SI_{Control\ at\ 1\ min} - SI_{Background\ at\ 1\ min})]$. To further quantify this effect, ^{125}I-labeled panitumumab was administered, organs of interest were excised, and radioactivity was measured 1 h postinjection. ^{125}I-Labeled panitumumab accumulated 27.5 ± 1.3% ID/g in PIT-treated tumors compared with 6.4 ± 0.5% ID/g in control tumors despite high blood pool activity (34.4 ± 2.1% ID/g) (Figure S1 in the Supporting Information), which was consistent with Pan-IR800 fluorescence imaging (Figure 1B). Only a slight increase of signal intensity was observed in the control tumors, especially when exposed to higher energy of light, probably because of scattered NIR light that crossed from the irradiated side through the body of the mouse (Figure 1C). A pathological study revealed that necrotic cell death in PIT-treated tumors was more intense when exposed to high-dose NIR light (Figure 1D). Although increased tumor damage was seen at light doses of more than 50 J/cm^2, we chose 50 J/cm^2 as an effective light dose for further *in vivo* experiments to avoid thermal effects of light therapy. In microscopy studies, secondary administration of fluorescence-labeled panitumumabs quickly diffused into the necrotic regions and bound to surviving A431 tumor cells within 24 h, demonstrating enhanced retention uniformly within the tumor bed (Figure S2). In contrast, nontargeted trastuzumab cleared from PIT-treated tumors within 24 h, although it could also be observed to spread throughout the tumor tissue much like panitumumab. Interestingly, the enhanced permeability of Pan-IR800 was maximal at 1 h after PIT and then

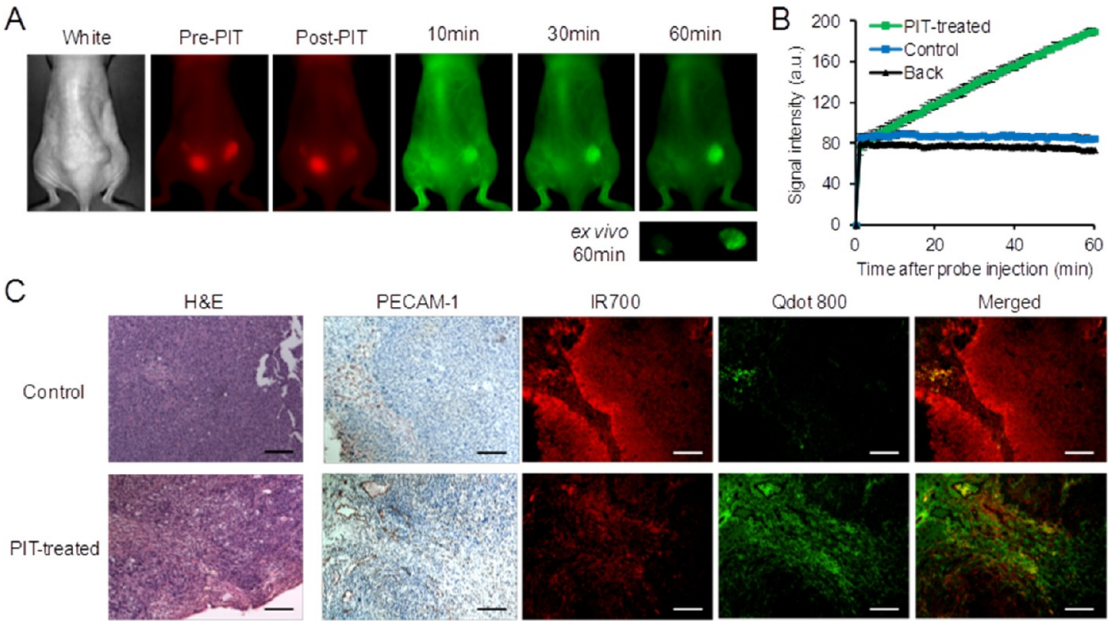

Figure 2. Enhanced permeability following PIT. (A) Dynamic images obtained after Qdot800 administration, one hour following Pan-IR700-mediated PIT. IR700: red, Qdot800: green. (B) Dynamic fluorescence intensity curve in the PIT-treated tumors, control tumors, and normal tissue with time. Data are means ± SEM (n = 4). (C) Histological analyses and fluorescence microscopy after PIT. PIT resulted in large areas of necrotic cell death as indicated by hematoxylin and eosin (H&E) staining. In the control tumor, Pan-IR700 accumulated only along the blood vessels (PECAM-1 staining), and little signal from Qdot800 was observed outside the blood vessels. However, within PIT-treated tumors, Qdot800 was broadly distributed within the necrotic regions and interstitium. IR700: red, Qdot800: green. Scale bars: 200 μm.

gradually decreased, returning to baseline by 24 h after PIT probably due to tissue repair processes of necrotic perivascular tumor cells that might recover tumor interstitial pressure (Figure S3). These results suggested that the optimal time to achieve maximal concentration of Pan-IR800 within the tumor is immediately after the PIT; however, increased uptake can still be observed up to 6 h after PIT, whereupon there is a steady decline in leakage to 24 h. There is a growing list of approved monoclonal antibodies targeting cancer antigens[13,14] that are amenable to conjugation with IR700 and, thus, are PIT candidate agents. Similar experiments with two different mAbs (panitumumab and trastzumab) against three different cells (A431 (HER1 positive), 3T3/HER2 (HER2 positive), and MDA-MB-468 (HER1 positive)) validated that super-enhanced permeability and retention (SUPR) effects occur regardless of the targeting antibodies and tumor cell lines employed (Figure S4). These results suggested that PIT could be a generally applicable method to dramatically enhance vascular permeability following light exposure (690 nm wavelength, at 50 J/cm^2), leading to the massive leakage of nanosized reagents (including nontargeted vehicles) in tumors.

PIT-Enhanced Delivery of Nontargeted Nanoparticles in Tumors. In order to validate the SUPR effect after PIT using nontargeted nanoparticles of larger size than antibodies, the pharmacokinetics of nontargeted PEGylated quantum dots (Qdot800; emission wavelength 800 nm, mean diameter 50 nm) were evaluated in A431 (HER1 positive)-bearing mice treated with Pan-IR700 PIT. Qdot800 was administered intravenously 1 h after light irradiation, and *in vivo* dynamic imaging studies were carried out. Rapid accumulation of Qdot800 was observed in the PIT-treated tumors immediately after injection, while uptake in the control tumor was minimal (Figure 2A and Video S2). The rate of increase in signal intensity between 1 and 60 min p.i. was 25.7-fold higher in the PIT-treated tumor than in the control tumor (Figure 2B). *Ex vivo* fluorescence imaging demonstrated the highest accumulation of Qdot800 in the PIT-treated tumors compared with other tissues including liver and lung 1 h p.i. (Figure S5). The Qdot800 signals in PIT-treated tumors were highly maintained up to 6 h p.i. (Figure S6), indicating prolonged retention relative to controls. A pathological analysis of harvested tumors demonstrated severe necrosis, creating a potential space for the Qdots to fill and surround residual viable cells (Figure 2C). PECAM-1 staining demonstrated that most of the interstitial tumor vessels in the PIT-treated tumors were dilated and the perivascular tumor cells were severely damaged (Figure 2C). Well-packed viable A431 cells labeled with fluorescence signals from Pan-IR700 binding were shown in the control tumors especially in perivascular tumor cells. In the control tumors, the fluorescence signals of Qdot800 were confined to the blood vessels. In summary, nontargeted Qdot800 of 50 nm in size extensively permeate into PIT-treated tumors 1 h after PIT.

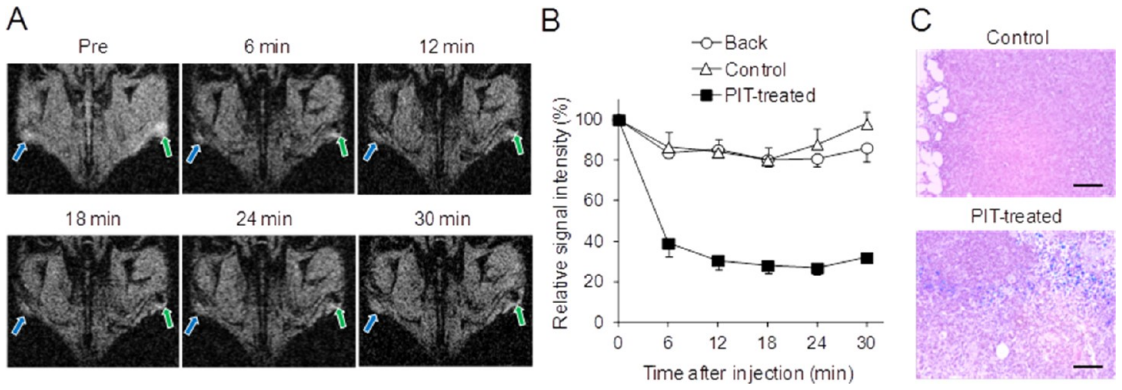

Figure 3. Intratumoral leakage of large nanoparticles (~200 nm) following PIT. (A) Dynamic T2*-weighted MRI images of SPIO after PIT indicate the selective uptake of SPIO in PIT-treated tumors (green arrow). Control tumor is indicated by blue arrow. Loss of signal indicates accumulation of the SPIO on MRI (right flank, green arrow). (B) Dynamic change of relative signal intensity in PIT-treated tumors, control tumors, and background. Data are means ± SEM (n = 3). (C) Massive uptake of SPIO (blue spots) within PIT-treated tumors was confirmed with Prussian blue staining. Scale bars: 200 μm.

Antibodies and antibody conjugates generally first bind to the perivascular target cells, as this is the layer of cells encountered immediately after extravasation from the feeding vessel. High-affinity binding can lead to trapping of the antibody in the perivascular space, which actually inhibits deeper penetration of the antibody into the tumor, a phenomenon known as the "binding site barrier".[15,16] Thus, the layer of tightly packed cells in the immediate perivascular space is most vulnerable to PIT. Upon exposure to NIR light, PIT induces immediate cytotoxic effects to these layers of cancer cells, resulting in a sudden perivascular necrosis and loss of vessel integrity. Following PIT, the vessels are patent but dilated due to the reduced tissue interstitial pressure. This results in dramatic increases in vascular permeability, which initially leads to extravasation into the perivascular space but ultimately deposits extravasated material throughout the tumor bed.

Maximum Size of Nanoparticles Delivered to Tumors after PIT. In order to test whether the SUPR effect could be observed with larger nanoparticles, we administered a superparamagnetic iron oxide (SPIO) (mean diameter ~200 nm) to tumor-bearing animals post-PIT and scanned animals using magnetic resonance imaging (MRI). SPIOs are MRI contrast agents that are rapidly taken up by the liver and have short circulation times in the blood, leading to low arterial input functions, normally resulting in minimal delivery to tumors.[17] Using dynamic T2* weighted MRI at 3 T, approximately 6 min after injection of the SPIO, the signal intensity in the PIT-treated tumors was dramatically reduced, while there was only a minimal decrease in signal in the control tumors, indicating that SPIO was accumulating preferentially in PIT-treated tumors (Figure 3A, B). The rate of decline in SI (indicating accumulation of SPIO) over 30 min was higher in the PIT-treated tumors than in control tumors (Figure 3B). At histology, SPIOs, detected by Prussian blue staining for iron, accumulated in the necrotic regions and within the interstitium of PIT-treated tumors (Figure 3C). These results demonstrated that nanoparticles of up to 200 nm in diameter could exhibit massive and rapid leakage into tumor tissues treated by PIT despite the rapid plasma clearance of SPIO.

The SUPR effect induced by PIT does not depend on specific characteristics of nanomaterials. Similar results were obtained with a T1-weighted contrast agent, gadolinium (Gd)-labeled polyamidoamine dendrimer (sixth generation) (G6-Gd, mean diameter = 10 nm[18]), and a T2*-weighted ultrasmall paramagnetic iron oxide contrast agent (USPIO, mean diameter = 20 nm[19]) (Figure S7). G6-Gd irregularly enhanced the interstitium of PIT-treated tumors, while only the rim of the control tumors was enhanced. The rate of increase in SI (indicating enhanced T1 relaxivity) between 2 and 30 min was 6.4-fold higher in the PIT-treated tumor than in the control tumor (Figure S7 and Video S3). USPIO was also rapidly taken up by PIT-treated tumors especially in the necrotic regions, as suggested by Prussian blue staining (Figure S7). These results prompted us to investigate whether liposomal chemotherapies might also exhibit the SUPR effect.

PIT-Enhanced Delivery and Efficacy of Anticancer Drugs. In order to examine the potential of PIT to increase the effectiveness of existing macromolecular therapeutic agents for cancer therapy, commercially available liposomal daunorubicin (DaunoXome; DX, mean diameter 50 nm) was administered to tumor-bearing mice in a therapy experiment. On the basis of its inherent fluorescence, optical imaging showed DX rapidly accumulated and diffused in PIT-treated tumors by 1 h (Figure 4A, B and Video S4). The ratio of fluorescence signal intensities at 60 min was 12.3-fold higher in the PIT-treated tumor compared with the control tumor using the following equation: $(SI_{PIT\ at\ 60\ min} - SI_{Background\ at\ 60\ min})/(SI_{Control\ at\ 60\ min} - SI_{Background\ at\ 60\ min})$ (Figure 4C). Similar to the Qdot800, which is of similar diameter,

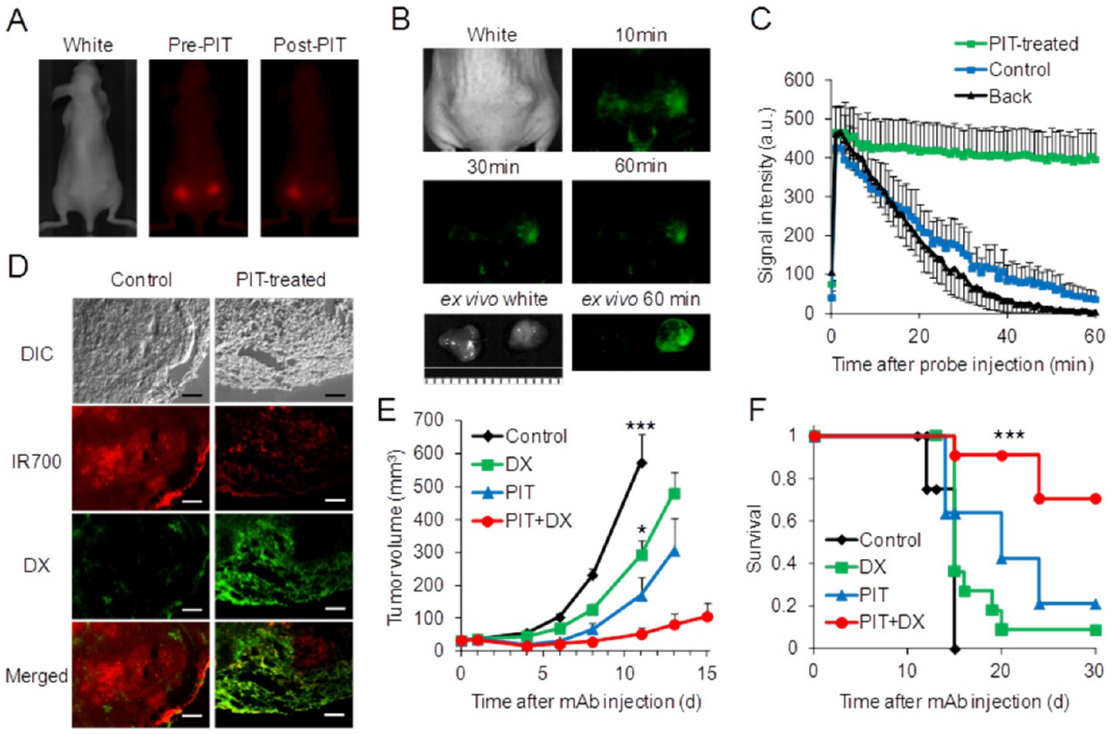

Figure 4. Therapeutic effect induced by the combination of PIT and liposomal daunorubicin. (A) *In vivo* fluorescence images of Pan-IR700 (red). PIT was performed only on the right-side tumor. (B) Liposomal daunorubicin (green) preferentially accumulated in PIT-treated tumors. The smallest scale bar indicates 1 mm. (C) Dynamic fluorescence intensity curves show that daunorubicin was taken up and retained by PIT-treated tumors selectively. "Back" shows the fluorescence in the back represents a background signal. Data are means ± SEM ($n = 4$). (D) Intratumoral localization of daunorubicin. Daunorubicin was broadly distributed encircling the surviving tumor cells in PIT-treated tumors. IR700: red, DX (DaunoXome): green. Scale bars: 200 μm. (E) Tumor growth inhibition by a combination therapy of Pan-IR700-mediated PIT and liposomal daunorubicin in A431 tumors. Data are means ± SEM ($n \geq 10$ mice in each group, ***$p < 0.001$, *$p < 0.05$ for treatment compared to control and DX-only groups using a Kruskal–Wallis test with post-testing). (F) Analysis using a Kaplan–Meier survival curve of the combination therapy of PIT and liposomal daunorubicin in A431 tumors ($n \geq 10$ mice in each group, ***$p < 0.05$ for treatment compared to the other control groups using a log-rank test with a Bonferroni's correction for multiple comparisons).

DX was widely distributed within the tumor, encircling the surviving tumor tissues, whereas the signals arising from DX in control tumors were confined to the immediate vicinity of the tumor blood vessels (Figure 4D). DX was highly retained in PIT-treated tumors for at least 24 h and co-localized with IR700 (indicating surviving tumor cells) especially after 6 h p.i. (Figure S8). This phenomenon was demonstrated both at the margin and within the core of the tumors (Figure S9).

A431 tumors were treated with a single dose of light (50 J/cm^2) 1 d after injection of Pan-IR700. We studied four groups of A431 tumor-bearing mice ($n \geq 10$ in each group) including PIT only, DX only, PIT + DX, and controls. All the treated tumors had a volume of less than 750 mm^3, in accordance with our institution's humane use of animals policy. Tumor volume was significantly reduced in A431 tumors treated with the combination of PIT + DX compared to untreated control mice and mice treated with DX only (Figure 4E), and survival was significantly prolonged in mice treated with PIT + DX compared to the other groups (Figure 4F). No obvious loss of body weight or systemic side effects were observed in the PIT + DX group (Figure S10). In this therapeutic study, more than a 10-fold increase in the concentration of Daunoxome can be achieved following PIT, leading to the killing of cells that survived the initial PIT. This dramatically enhanced permeability, named the SUPR effect (Figure 5), may be unique to PIT because, compared with other conventional cancer therapies, which induce cell death through slower, apoptotic pathways, the effects of PIT are immediate and massive, and thus, there is a sudden increase in permeability and retention, which is ideal for combinatorial cancer therapy, especially involving nanosized agents. Other attempts have been made to augment the EPR effect with nitroglycerin (nitric oxide releasing agent),[20−22] angiotensin II,[22,23] and gold nanoparticle[24,25] for enhanced permeability of tumor vasculature by targeting the normal vasculature or endothelial cells, and these methods could be combined with SUPR effects. Furthermore, the SUPR effect induced by PIT leads to increased permeability of anticancer reagents deep into the tumor. Therefore, the SUPR effect might enable more homogeneous distribution of high concentrations of anticancer drugs that would prevent the recurrence of cancer after PIT alone, which might occur

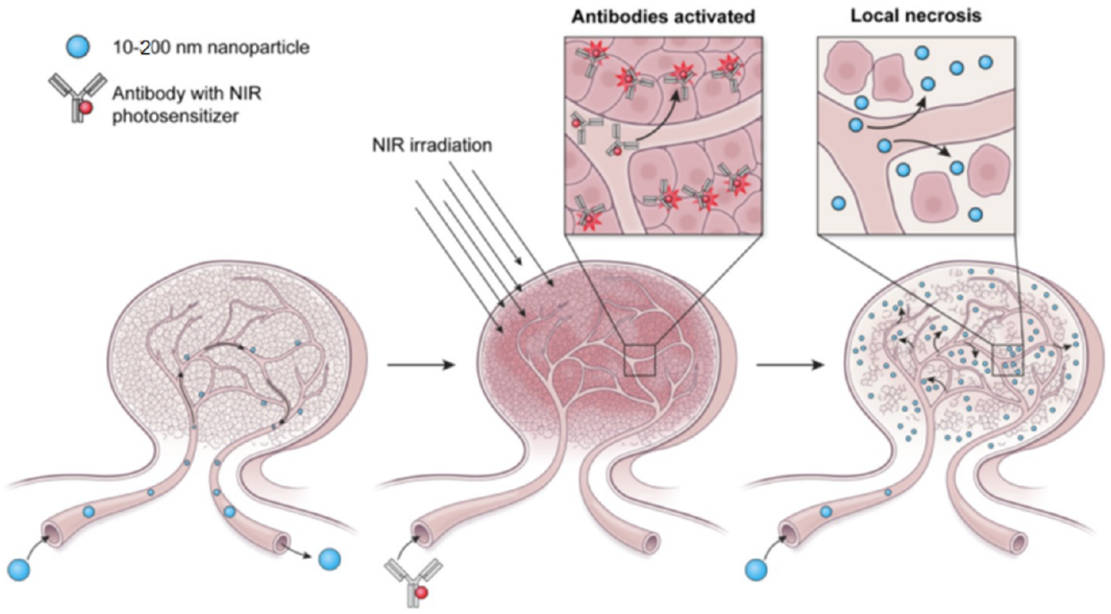

Figure 5. Concept of the super-enhanced permeability and retention (SUPR) effect for explaining PIT-mediated enhancement of nanodrug delivery. Although most nanoparticles remain intravascular without retention in control tumors, target-specific PIT induces a profound perivascular cell death, leading to the massive leakage of nanoparticles into the tumor bed.

due to inhomogeneous antigen expression and antibody distribution in human cancers.

CONCLUSIONS

PIT results in a sudden increase in vascular permeability that allows nanosized particles to extravasate rapidly into the treated tumor bed, leading to super-enhanced permeability and retention. This process is most marked in the first 6 h after PIT but becomes less pronounced afterward, reaching baseline levels by 24 h. Thus, there is a limited window during which nanosized particles could be administered to augment the effects of PIT, thus greatly augmenting the effectiveness of PIT alone. The combination of PIT and nanosized drug delivery holds promise for maximizing cancer cell killing while minimizing nontarget side effects associated with conventional anticancer drugs.

METHODS

Cell Lines and Culture. A431 cells expressing HER1 were used for PIT. Cells were grown in RPMI1640 supplemented with 10% FBS and 1% penicillin–streptomycin in tissue culture flasks in a humidified incubator at 37 °C in an atmosphere of 95% air and 5% carbon dioxide.

Synthesis of Dye-Conjugated MAbs. Conjugation of dyes with mAbs was performed according to the procedure reported previously.[11] Each mAb (1 mg, 6.8 nmol) was incubated with IRDye 700DX NHS ester (LI-COR Biosciences, Lincoln, NE, USA) (60.2 μg, 30.8 nmol) or IRDye 800CW NHS ester (LI-COR Biosciences) (35.9 μg, 30.8 nmol) in 0.1 M Na_2HPO_4 (pH 8.6) at room temperature for 1 h. The mixture was purified with a Sephadex G50 column (PD-10; GE Healthcare). The concentration of dye and protein was measured by absorption with spectroscopy (8453 Value System; Agilent Technologies) to confirm the number of fluorophore molecules conjugated to each mAb molecule. The number of IR700 and IR800 per antibody was adjusted to approximately four and two, respectively.

***In Vivo* Nanodrug Delivery after Photoimmunotherapy.** All *in vivo* procedures were conducted in compliance with the Guide for the Care and Use of Laboratory Animal Resources (1996), U.S. National Research Council, and approved by the National Cancer Institute/NIH Animal Care and Use Committee. Six-week-old to 8-week-old female homozygote athymic nude mice were purchased from Charles River (National Cancer Institute, Frederick). During treatment, mice were anesthetized with isoflurane. Two million A431 cells were injected subcutaneously in the right and left flanks of each mouse. Five days after cell injection, 100 μg of Pan-IR700 was administered intravenously, and 1 day later, one side was irradiated with NIR light from a red-light-emitting diode at wavelengths of 670–710 nm and a power density of 10–100 J/cm^2, as measured with an optical power meter (PM 100 (Thorlabs)). The other side was shielded from light using aluminum foil. One hour after PIT, Pan-IR800 (100 μg), pegylated nontargeted quantum dots (Qtracker 800 nontargeted quantum dots; Qdot800) (32.5 pmol), or liposomal daunorubicin (DaunoXome; DX) (30 mg/kg) was injected intravenously, and *in vivo* dynamic imaging studies were carried out.

In vivo fluorescence images of IR700 and IR800 were obtained with a Pearl Imager (LI-COR Biosciences) using the 700 and 800 nm fluorescence channel. Qdot800 was detected with Maestro *in vivo* Imaging System (CRi Inc., Woburn, MA, USA) using a band-pass filter, which ranges between 575 and 605 nm (excitation), and a long-pass NIR filter over 800 nm (emission). Fluorescence images of daunorubicin were also obtained with Maestro using a band-pass filter from 503 to 555 nm (excitation) and a long-pass green filter over 580 nm (emission). The tunable emission filter was automatically stepped in 10 nm increments from 650 to 950 nm and from 500 to 800 nm for the NIR and green filter sets at constant exposure. The spectral fluorescence images consist of autofluorescence spectra and the spectra from Qdot800 and daunorubicin, which were then unmixed, based on their spectral patterns using commercial software (Maestro software; CrI Inc.).

For MR imaging, SPIO (Feridex, 30 mg/kg) was administered intravenously 1 h post-PIT, and dynamic contrast-enhanced MR images for 30 min were obtained with an Intera Achieva 3.0 T clinical scanner (Philips Medical Systems) using an in-house dedicated mouse receiver coil. SPIO was used as a negative contrast agent on T2-weighted images. T2-weighted image sequences were applied in the coronal. For iron imaging, fast field echo imaging (T2-FFE) was employed (TR/TE = 277.7/9.23 ms, flip angle = 20°, matrix = 512 × 256, FOV = 70 × 70 mm, coronal slice = 67, slice thickness = 0.20 mm, NSA = 6, scan time = ~5.5 min) with optimal TE time, in which tumors were seen as bright lesions before PIT. For administration of these agents, a 30-gauge needle was placed into the tail vein and extended using Tygon tubing (0.01 in. internal diameter). During the measurements, the breathing rates of the mice were monitored using a Biopac System MP150 (Biopac Inc.). Respiration rate was maintained at 25−30 respirations per min. Before intravenous injection of each agent, plain images were obtained with T2-weighted image sequences as previously described. After bolus injection of each agent at the amount of 100 μL, a sequential DCE MRI series was acquired for ~30 min with the same sequence. The tumors were excised and frozen or paraffin-embedded for histological study, fluorescence microscopy study, and Prussian blue staining after *ex vivo* imaging.

Therapeutic Study Based on SUPR Effect Using Liposomal Daunorubicin. To determine the effectiveness of PIT and DaunoXome, the following experiment was conducted: One million A431 cells were injected subcutaneously in the right flank of the mice. In order to determine the tumor volume, the greatest longitudinal diameter (length) and the greatest transverse diameter (width) were determined with an external caliper. Tumor volume based on caliper measurements was calculated using the following formula: tumor volume = length × width^2 × 0.5.[26] Tumors reaching approximately 40 mm^3 in volume were selected for the study. Selected mice were randomized into 4 groups of at least 10 mice per group for the following treatments: (1) no treatment; (2) liposomal daunorubicin (6 mg/kg); (3) PIT (50 J/cm^2); (4) PIT (50 J/cm^2), followed by liposomal daunorubicin (6 mg/kg) 1 h later. After treatment, the mice were monitored daily, and their tumor volume was measured twice a week until it reached 750 mm^3, at which time mice were euthanized with carbon dioxide gas.

Fluorescence Microscopy. Frozen or paraffin sections 10 μm thick were prepared, and fluorescence was assessed using an Olympus BX51 microscope (Olympus America, Inc., Melville, NY, USA) equipped with the following filters: excitation wavelength 590 to 650 nm, 360 to 370 nm, and 480 to 550 nm, emission wavelength 662.5 to 747.5 nm, 765 to 855 nm, and 590 nm long pass for IR700, Qdot800, and daunorubicin, respectively. Transmitted light differential interference contrast images were also acquired. Hematoxylin and eosin (H&E) staining, platelet/endothelial cell adhesion molecule-1 (PECAM-1) immunohistochemical staining, and Prussian blue staining were performed according to standard protocol.

Statistical Analysis. Data are expressed as means ± SEM from a minimum of three experiments, unless otherwise indicated. Statistical analyses were carried out using a statistics program (GraphPad Prism; GraphPad Software). For multiple comparisons, a one-way analysis of variance (ANOVA) with post test (Kruskal−Wallis test with post-test) was used. The cumulative probability of survival, determined herein as the tumor volume failed to reach 750 mm^3, was estimated in each group with the use of the Kaplan−Meier survival curve analysis, and the results were compared with use of the log-rank test with Bonferroni's correction for multiple comparisons. $p < 0.05$ was considered to indicate a statistically significant difference.

Conflict of Interest: The authors declare no competing financial interest.

Acknowledgment. This research was supported by the Intramural Research Program of the U.S. National Institutes of Health, National Cancer Institute, Center for Cancer Research.

Supporting Information Available: Extensive methods section; biodistribution of radiolabeled antibody after PIT (Figure S1); target-specific binding of antibody to surviving tumor cells after PIT (Figure S2); optimal timing of maximam nanodrug accumulation in tumors after PIT (Figure S3); feasibility of SUPR effect for various cancer cell lines (Figure S4); *ex vivo* fluorescence imaging after PIT (Figure S5); change of fluorescence signal of Qdot800 in PIT-treated tumors over time (Figure S6); SUPR effect with a variety of nanoparticulate MR contrast agents (Figure S7); intratumoral biodistribution and retention of liposomal daunorubicin in PIT-treated tumors (Figure S8); comparison of biodistribution of liposomal daunorubicin in the margin and core of tumors (Figure S9); body weight of tumor mice treated with liposomal daunorubicin 1 h after PIT (Figure S10); dynamic fluorescence imaging of Pan-IR800 in PIT-treated A431 tumors (Video S1); dynamic fluorescence imaging of Qdot800 in PIT-treated A431 tumors (Video S2); dynamic fluorescence imaging of G6-Gd in PIT-treated A431 tumors (Video S3); dynamic fluorescence imaging of liposomal daunorubicin in PIT-treated A431 tumors (Video S4). This material is available free of charge *via* the Internet at http://pubs.acs.org.

REFERENCES AND NOTES

1. Minchinton, A. I.; Tannock, I. F. Drug Penetration in Solid Tumours. *Nat. Rev. Cancer* **2006**, *6*, 583–592.
2. Hambley, T. W.; Hait, W. N. Is Anticancer Drug Development Heading in the Right Direction? *Cancer Res.* **2009**, *69*, 1259–1262.
3. Peer, D.; Karp, J. M.; Hong, S.; Farokhzad, O. C.; Margalit, R.; Langer, R. Nanocarriers as an Emerging Platform for Cancer Therapy. *Nat. Nanotechnol.* **2007**, *2*, 751–760.
4. Maeda, H. Tumor-Selective Delivery of Macromolecular Drugs *via* the EPR Effect: Background and Future Prospects. *Bioconjugate Chem.* **2010**, *21*, 797–802.
5. Maeda, H.; Matsumura, Y. EPR Effect Based Drug Design and Clinical Outlook for Enhanced Cancer Chemotherapy. *Adv. Drug Delivery Rev.* **2011**, *63*, 129–130.
6. Vicent, M. J.; Duncan, R. Polymer Conjugates: Nanosized Medicines for Treating Cancer. *Trends Biotechnol.* **2006**, *24*, 39–47.
7. Jain, R. K. The Next Frontier of Molecular Medicine: Delivery of Therapeutics. *Nat. Med.* **1998**, *4*, 655–657.
8. Vaage, J.; Donovan, D.; Mayhew, E.; Abra, R.; Huang, A. Therapy of Human Ovarian Carcinoma Xenografts Using Doxorubicin Encapsulated in Sterically Stabilized Liposomes. *Cancer* **1993**, *72*, 3671–3675.
9. Forssen, E. A.; Coulter, D. M.; Proffitt, R. T. Selective *in Vivo* Localization of Daunorubicin Small Unilamellar Vesicles in Solid Tumors. *Cancer Res.* **1992**, *52*, 3255–3261.
10. Presant, C. A.; Scolaro, M.; Kennedy, P.; Blayney, D. W.; Flanagan, B.; Lisak, J.; Presant, J. Liposomal Daunorubicin Treatment of HIV-Associated Kaposi's Sarcoma. *Lancet* **1993**, *341*, 1242–1243.
11. Mitsunaga, M.; Ogawa, M.; Kosaka, N.; Rosenblum, L. T.; Choyke, P. L.; Kobayashi, H. Cancer Cell-Selective *in Vivo* Near Infrared Photoimmunotherapy Targeting Specific Membrane Molecules. *Nat. Med.* **2011**, *17*, 1685–1691.
12. Giusti, R. M.; Shastri, K.; Pilaro, A. M.; Fuchs, C.; Cordoba-Rodriguez, R.; Koti, K.; Rothmann, M.; Men, A. Y.; Zhao, H.; Hughes, M.; *et al.* U.S. Food and Drug Administration Approval: Panitumumab for Epidermal Growth Factor Receptor-Expressing Metastatic Colorectal Carcinoma with Progression Following Fluoropyrimidine-, Oxaliplatin-, and Irinotecan-Containing Chemotherapy Regimens. *Clin. Cancer Res.* **2008**, *14*, 1296–1302.
13. Waldmann, T. A. Immunotherapy: Past, Present, and Future. *Nat. Med.* **2003**, *9*, 269–277.
14. Reichert, J. M.; Rosensweig, C. J.; Faden, L. B.; Dewitz, M. C. Monoclonal Antibody Successes in the Clinic. *Nat. Biotechnol.* **2005**, *23*, 1073–1078.
15. Weinstein, J. N.; Eger, R. R.; Covell, D. G.; Black, C. D.; Mulshine, J.; Carrasquillo, J. A.; Larson, S. M.; Keenan, A. M. The Pharmacology of Monoclonal Antibodies. *Ann. N.Y. Acad. Sci.* **1987**, *507*, 199–210.
16. Weinstein, J. N.; van Osdol, W. Early Intervention in Cancer Using Monoclonal Antibodies and Other Biological

Ligands: Micropharmacology and the "Binding Site Barrier". *Cancer Res.* **1992**, *52*, 2747s–2751s.
17. Weissleder, R.; Stark, D. D.; Engelstad, B. L.; Bacon, B. R.; Compton, C. C.; White, D. L.; Jacobs, P.; Lewis, J. Superparamagnetic Iron Oxide: Pharmacokinetics and Toxicity. *AJR Am. J. Roentgenol.* **1989**, *152*, 167–173.
18. Kobayashi, H.; Brechbiel, M. W. Nanosized MRI Contrast Agents with Dendrimer Cores. *Adv. Drug Delivery Rev.* **2005**, *57*, 2271–2286.
19. Clarke, S. E.; Weinmann, H. J.; Dai, E.; Lucas, A. R.; Rutt, B. K. Comparison of Two Blood Pool Contrast Agents for 0.5-T MR Angiography: Experimental Study in Rabbits. *Radiology* **2000**, *214*, 787–794.
20. Seki, T.; Fang, J.; Maeda, H. Enhanced Delivery of Macromolecular Antitumor Drugs to Tumors by Nitroglycerin Application. *Cancer Sci.* **2009**, *100*, 2426–2430.
21. Maeda, H. Nitroglycerin Enhances Vascular Blood Flow and Drug Delivery in Hypoxic Tumor Tissues: Analogy between Angina Pectoris and Solid Tumors and Enhancement of the EPR Effect. *J. Controlled Release* **2010**, *142*, 296–298.
22. Maeda, H. Macromolecular Therapeutics in Cancer Treatment: The EPR Effect and Beyond. *J. Controlled Release* **2012**, *164*, 138–144.
23. Suzuki, M.; Hori, K.; Abe, I.; Saito, S.; Sato, H. A New Approach to Cancer Chemotherapy: Selective Enhancement of Tumor Blood Flow with Angiotensin II. *J. Natl. Cancer Inst.* **1981**, *67*, 663–669.
24. El-Sayed, I. H.; Huang, X.; El-Sayed, M. A. Selective Laser Photo-Thermal Therapy of Epithelial Carcinoma Using Anti-EGFR Antibody Conjugated Gold Nanoparticles. *Cancer Lett.* **2006**, *239*, 129–135.
25. Gormley, A. J.; Larson, N.; Sadekar, S.; Robinson, R.; Ray, A.; Ghandehari, H. Guided Delivery of Polymer Therapeutics Using Plasmonic Photothermal Therapy. *Nano Today* **2012**, *7*, 158–167.
26. Euhus, D. M.; Hudd, C.; LaRegina, M. C.; Johnson, F. E. Tumor Measurement in the Nude Mouse. *J. Surg. Oncol.* **1986**, *31*, 229–234.